Applied Physics Letters

Revealing topological attributes of stiff plates by Dirac factorization of their 2D elastic wave equation

Cite as: Appl. Phys. Lett. **120**, 081701 (2022); https://doi.org/10.1063/5.0086559
Submitted: 26 January 2022 • Accepted: 09 February 2022 • Published Online: 22 February 2022

P. A. Deymier and K. Runge

Applied Physics Letters ARTICLE scitation.org/journal/apl

Revealing topological attributes of stiff plates by Dirac factorization of their 2D elastic wave equation

Cite as: Appl. Phys. Lett. **120**, 081701 (2022); doi: 10.1063/5.0086559
Submitted: 26 January 2022 · Accepted: 9 February 2022 ·
Published Online: 22 February 2022

P. A. Deymier[a] and K. Runge

AFFILIATIONS

Department of Materials Science and Engineering, The University of Arizona, Tucson, Arizona 85721, USA

Note: This paper is part of the APL Special Collection on Acoustic and Elastic Metamaterials and Metasurfaces.
[a]**Author to whom correspondence should be addressed:** deymier@arizona.edu

ABSTRACT

Dirac factorization of the elastic wave equation of two-dimension stiff plates coupled to a rigid substrate reveals the possible topological properties of elastic waves in this system. These waves may possess spin-like degrees of freedom associated with a gapped band structure reminiscent of the spin Hall effect. In semi-infinite plates or strips with zero displacement edges, the Dirac-factored elastic wave equation shows the possibility of edge modes moving in opposite directions. The finite size of strips leads to overlap between edge modes consequently opening a gap in their spectrum eliminating the spin Hall-like effects. This Dirac factorization tells us what solutions of the elastic wave equation would be if we could break some symmetry. Dirac factorization does not break symmetry but simply exposes what topological properties of elastic waves may result from symmetry breaking structural or external perturbations.

Topological acoustics (TA) is revolutionizing the field of acoustic and elastic waves.[1] Simple one-dimensional (1D) phononic structures, analogous to the condensed matter Su–Schrieffer–Heeger (SSH) model, have revealed many of the fundamental properties of TA waves, such as nontrivial topological invariants (e.g., Chern number), edge states at surfaces and interfaces between topologically different media, and bulk-boundary correspondence.[2–5] The latter is a powerful guide to design topologically protected edge modes,[6] whereby the number of edge modes is the difference in Chern number between those topological phases sharing an interface. In the SSH model, parity symmetry is broken intrinsically through a system's structure. Spatiotemporal modulations of the elastic properties of 1D phononic structures can break time-reversal and parity symmetry.[7–10] Two- (2D) or three-dimensional (3D) TA systems have exploited analogies with the quantum Hall effect (QHE),[11] the quantum spin Hall effect (QSHE),[12] and the quantum valley Hall effect (QVHE).[13] 2D TA systems use triangular-lattice or graphene-like structures that exhibit Dirac degeneracies in their band structure, and symmetry breaking opens a gap associated with a nontrivial topology. Breaking symmetry intrinsically (e.g., parity symmetry) leads to acoustic analogues of the QSHE or QHVE. Extrinsically breaking time-reversal symmetry results in acoustic analogues of the QHE. 3D acoustic and mechanical metamaterials have demonstrated Weyl points and Fermi arc-like surface states.[14–17] The hallmark of spin Hall insulators is the presence of gapless edge states with different "spins" moving in opposite directions that may lead to immunity to backscattering.

The Dirac equation[18] has revealed the possibility of emergence of the spin degrees of freedom of the electron from relativistic effects. However, application of a magnetic field that breaks symmetry is necessary to observe the spin degrees of freedom.[19] In the same spirit, Dirac factorization of elastic wave equations in 1D systems composed of coupled elastic waveguides has revealed the possibility of the existence of pseudospin elastic waves, which amplitude takes the form of a spinor in the two-dimensional Hilbert space of the direction of propagation along the waveguide.[20–24] The Dirac factorization tells us what solutions of the elastic wave equation would be if we could break some symmetry. Dirac factorization does not break symmetry. One would need to add a structural or external perturbation to break symmetries and reveal Dirac-like solutions, such as is done in the models of spin Hall insulators described above.

In this paper, we extend the approach of Dirac factorization of elastic wave equations to 2D. The elastic wave equation for a stiff string in the absence of shear stress and rotational inertia is given by the Euler–Bernoulli equation:[25]

$$\frac{\partial^2 u}{\partial t^2} = a^2 \frac{\partial^2 u}{\partial x^2} - b^2 \frac{\partial^4 u}{\partial x^4}, \tag{1}$$

where the first two terms are the usual terms for the motion of a vibrating string and the third term is due to the resistance of the stiff string to bending. Here, a and b are the longitudinal speed of sound and a coefficient dependent on the cross-sectional area and the radius of gyration of the string, Young's modulus and linear density of the constitutive material. x is the direction along the string. Generalization of this equation to wave propagation in an isotropic homogeneous thin plate takes the form of Kirchhoff–Love equation:[26]

$$\frac{\partial^2 u}{\partial t^2} = A^2 \frac{\partial^2 u}{\partial x^2} + A^2 \frac{\partial^2 u}{\partial y^2} - B^2 \left(\frac{\partial^4 u}{\partial x^4} + 2 \frac{\partial^4 u}{\partial x^2 \partial x^2} + \frac{\partial^4 u}{\partial y^4} \right). \tag{2}$$

Again, A is the speed of sound and B depends on the thickness of the plate, Young's modulus, and Poisson ratio. x, y are orthogonal directions in the plane of the plate.

If the plate is elastically coupled to a rigid substrate through some medium, an additional restoring force arises and the wave equations now take the form:

$$\frac{\partial^2 u}{\partial t^2} = A^2 \frac{\partial^2 u}{\partial x^2} + A^2 \frac{\partial^2 u}{\partial y^2} - M^2 u - B^2 \left(\frac{\partial^4 u}{\partial x^4} + 2 \frac{\partial^4 u}{\partial x^2 \partial x^2} + \frac{\partial^4 u}{\partial y^4} \right). \tag{3}$$

In Eq. (3), M^2 represents the stiffness of the additional restoring force due to the coupling medium.

This equation can be rewritten algebraically as

$$Hu = \left\{ C^2 \frac{\partial^2}{\partial x^2} + C^2 \frac{\partial^2}{\partial y^2} - \left(M + B \left(\frac{\partial^2}{\partial x^2} + \frac{\partial^2}{\partial y^2} \right) \right)^2 - \frac{\partial^2}{\partial t^2} \right\} u = 0, \tag{4}$$

with $C^2 = A^2 + 2MB$. In Eq. (4), the displacement u is a scalar quantity.

The differential operator, H, of Eq. (4) is redefined as a 2×2 diagonal matrix so that it can be conveniently Dirac factored[18] recovering the familiar Dirac forms. More specifically, we can write that equation in the form of the subsequent application of two matrix differential operators to a vector-like displacement, namely, $H^- H^+ \boldsymbol{u} = 0$ where the differential operators $H^\pm$ are given by

$$H^\pm = -iC \frac{\partial}{\partial x} \boldsymbol{\sigma_x} - iC \frac{\partial}{\partial y} \boldsymbol{\sigma_y} - \left(M + B \left(\frac{\partial^2}{\partial x^2} + \frac{\partial^2}{\partial y^2} \right) \right) \boldsymbol{\sigma_z} \pm i \frac{\partial}{\partial t} \boldsymbol{I}. \tag{5}$$

In Eq. (5), $\boldsymbol{\sigma_x} = \begin{pmatrix} 0 & 1 \\ 1 & 0 \end{pmatrix}$, $\boldsymbol{\sigma_y} = \begin{pmatrix} 0 & -i \\ i & 0 \end{pmatrix}$, $\boldsymbol{\sigma_z} = \begin{pmatrix} 1 & 0 \\ 0 & -1 \end{pmatrix}$ are the Pauli matrices and $\boldsymbol{I} = \begin{pmatrix} 1 & 0 \\ 0 & 1 \end{pmatrix}$ is the identity matrix. i is the imaginary quantity $\sqrt{-1}$.

In contrast to H which satisfies time reversal and parity symmetries (i.e., one can replace t by $-t$ and/or $x(y)$ by $-x(-y)$ and retain the form of the equation), the operators, $H^\pm$, do not satisfy $x(y)$ parity symmetry. It satisfies time reversal symmetry as changing the sign of time simply changes the sign of the term $\pm i \frac{\partial}{\partial t} \boldsymbol{I}$. We note that solutions of the equations $H^\pm \boldsymbol{u} = 0$, where $\boldsymbol{u}$ is now a 2×1 vector, are solutions of Eq. (4). However, the reverse is not true. With the Dirac factorization $\boldsymbol{u}$ can be efficiently represented as a spinor.[27] This spinor represents the quasi-standing wave nature of solutions to Eq. (4), that is, it is a superposition of forward and backward going waves with different amplitudes dependent on the wave vector.

Let us now solve

$$H^- \boldsymbol{u} = 0. \tag{6}$$

We investigate here Eq. (6) only since H^+ is related to H^- by time reversal, and its solutions will be the time reversed solutions of Eq. (6).

We seek plane wave solutions of the form $\boldsymbol{u} = \begin{pmatrix} u_1 \\ u_2 \end{pmatrix} e^{ik_x x} e^{ik_y y} e^{i\omega t}$. Here, $\vec{k} = k_x$, k_y, and ω are a two-dimensional wave vector and the angular frequency. The operators $H^\pm$ are analogous to the long wavelength limit of the Qi, Wu, and Zhang (QWZ) model of the anomalous quantum Hall effect.[28] Indeed, the $\vec{k}$ dependent part of the operator $H^\pm$, namely, $H^\pm_{\vec{k}} = Ck_x \boldsymbol{\sigma_x} + Ck_y \boldsymbol{\sigma_y} - \left(M + B \left(-k_x^2 - k_y^2 \right) \right) \boldsymbol{\sigma_z}$ is the long wavelength limit of the QWZ-like operator, $H_{QWZ}(\vec{k}) = C \sin k_x \boldsymbol{\sigma_x} + C \sin k_y \boldsymbol{\sigma_y} + \left(-(M + 4B) + 2B \cos k_x + 2B \cos k_y \right) \boldsymbol{\sigma_z}$. This periodic model is a Chern insulator based on the Berry phase in $\vec{k}$ space.[29] In the long-wavelength limit, the topology of the Dirac-factored wave equation of the stiff plate is directly connected to the non-trivial topology of the QWZ-like model.

Inserting the plane wave solution into Eq. (6) yields the Eigen value problem,

$$D \begin{pmatrix} u_1 \\ u_2 \end{pmatrix} = \begin{pmatrix} X^- & Z^* \\ Z & X^+ \end{pmatrix} \begin{pmatrix} u_1 \\ u_2 \end{pmatrix} = 0, \tag{7}$$

where $X^\pm = \omega \pm \left(M - B \left(k_x^2 + k_y^2 \right) \right)$ and $Z = C \left(k_x + ik_y \right)$. Z^* is the complex conjugate of Z. One finds nontrivial solutions if the determinant of the matrix D is zero yielding the dispersion relation,

$$\omega^2 = \left(M - B \left(k_x^2 + k_y^2 \right) \right)^2 + C^2 \left(k_x^2 + k_y^2 \right). \tag{8}$$

This dispersion relation has a cutoff frequency at $k_x, k_y = 0$, at which point $\omega = \pm M$. There also exist evanescent modes within the gap $\omega \in [M, -M]$. Seeking evanescent modes in the y direction, we use solutions of Eq. (6), in the form $\boldsymbol{u} = \begin{pmatrix} u_1 \\ u_2 \end{pmatrix} e^{ik_x x} e^{\lambda y} e^{i\omega t}$ where λ is a real quantity. Inserting this form into Eq. (6) yields an eigenvalue problem $D' \begin{pmatrix} u_1 \\ u_2 \end{pmatrix} = 0$ where the components of the matrix D' are all real. The condition $detD' = 0$ for nontrivial solutions results in the dispersion relation for evanescent modes,

$$\omega^2 = \left(M - B \left(k_x^2 - \lambda^2 \right) \right)^2 + C^2 \left(k_x^2 - \lambda^2 \right). \tag{9}$$

Equation (9) can be used to solve for $\lambda(\omega)$. There are two solutions given by

$$\lambda_{1,2}^2 = k_x^2 + F \pm \sqrt{F^2 - \frac{(M^2 - \omega^2)}{B^2}}. \tag{10}$$

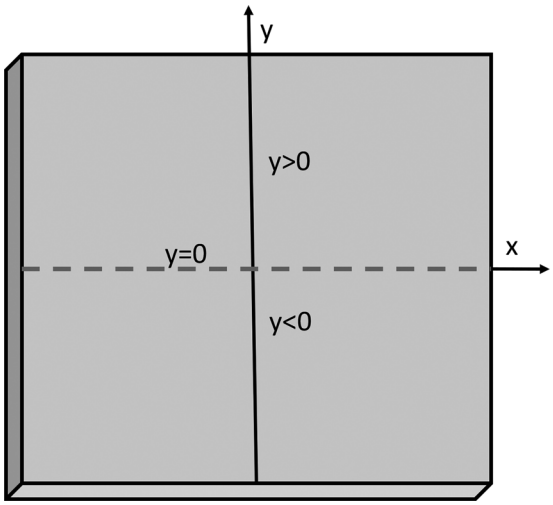

FIG. 1. Schematic illustration of the two semi-infinite plates $y > 0$ or $y < 0$ with zero displacement boundary condition along the $y = 0$ line (dashed line).

In that equation, $F = \frac{A^2}{2B^2}$.

We now consider the emergence of edge modes along a line with zero displacement cutting through the stiff plate at $y = 0$ (Fig. 1).

The stiff plate now is reduced to two semi-infinite plates with either $y > 0$ or $y < 0$. We seek linear combinations of evanescent solutions in y satisfying the boundary condition $\boldsymbol{u}(x, y = 0, \omega) = 0$. For this, we use the ansatz,

$$\boldsymbol{u} = \begin{pmatrix} u_1 \\ u_2 \end{pmatrix} e^{ik_x x}\left(e^{\lambda_1 y} - e^{\lambda_2 y}\right)e^{i\omega t}. \tag{11}$$

Inserting Eq. (11) into Eq. (6) leads to the eigenvalue problem,

$$D'' \begin{pmatrix} u_1 \\ u_2 \end{pmatrix} = \begin{pmatrix} N_- & Q_- \\ Q_+ & N_+ \end{pmatrix} \begin{pmatrix} u_1 \\ u_2 \end{pmatrix} = 0, \tag{12}$$

where

$$N_\pm = \omega f(\lambda_1, \lambda_2) \pm \left(\left(M - Bk_x^2\right) f(\lambda_1, \lambda_2) + Bg(\lambda_1, \lambda_2)\right), \tag{13a}$$

$$Q_\pm = C\left(k_x f(\lambda_1, \lambda_2) \pm h(\lambda_1, \lambda_2)\right), \tag{13b}$$

with $f(\lambda_1, \lambda_2) = e^{\lambda_1 y} - e^{\lambda_2 y}$, $g(\lambda_1, \lambda_2) = \lambda_1^2 e^{\lambda_1 y} - \lambda_2^2 e^{\lambda_2 y}$ and $h(\lambda_1, \lambda_2) = \lambda_1 e^{\lambda_1 y} - \lambda_2 e^{\lambda_2 y}$.

Nontrivial solutions arise when $det\, D'' = 0$. After some algebraic manipulations, this condition takes the form,

$$\begin{aligned} &\left[\omega^2 - \left(M - B\left(k_x^2 - \lambda_1^2\right)\right)^2 + C^2\left(k_x^2 - \lambda_1^2\right)\right] e^{2\lambda_1 y} \\ &+ \left[\omega^2 - \left(M - B\left(k_x^2 - \lambda_2^2\right)\right)^2 + C^2\left(k_x^2 - \lambda_2^2\right)\right] e^{2\lambda_2 y} \\ &+ \left[-2\omega^2 + 2\left(M - B\left(k_x^2 - \lambda_1^2\right)\right)\left(M - B\left(k_x^2 - \lambda_2^2\right)\right)\right. \\ &\left. + 2C^2\left(k_x^2 - \lambda_1\lambda_2\right)\right] e^{\lambda_1 y} e^{\lambda_2 y} = 0. \end{aligned}$$

The first two terms in square brackets vanish as they represent the dispersion relations of bulk evanescent modes [Eq. (9)]. The remaining term in the square bracket must then be identical to zero. Eliminating ω^2 by adding the three equations $\omega^2 - \left(M - B\left(k_x^2 - \lambda_1^2\right)\right)^2 + C^2\left(k_x^2 - \lambda_1^2\right) = 0$, $\omega^2 - \left(M - B\left(k_x^2 - \lambda_2^2\right)\right)^2 + C^2\left(k_x^2 - \lambda_2^2\right) = 0$, and $-2\omega^2 + 2\left(M - B\left(k_x^2 - \lambda_1^2\right)\right)\left(M - B\left(k_x^2 - \lambda_2^2\right)\right) + 2C^2\left(k_x^2 - \lambda_1\lambda_2\right) = 0$ and after some algebraic manipulations, we obtain

$$\left(\lambda_1 + \lambda_2\right)^2 = \frac{C^2}{B^2}. \tag{14a}$$

Using these three bracketed equations, we can also find

$$\lambda_1\lambda_2 = k_x^2 - \frac{2\omega^2 - 2M(M + BF)}{C^2}. \tag{14b}$$

These conditions on the edge states coefficients, λ_1 and λ_2, depend on the bulk dispersion relations and, therefore, fully reflect the long wavelength bulk topological properties of the plate.

Finally, combining Eqs. (14a) and (14b) and Eq. (10), we find that

$$\omega^2 = C^2 k_x^2. \tag{14c}$$

There are, therefore, two possible branches for evanescent modes in the y direction, namely, $\omega = \pm Ck_x$. The first branch corresponds to an evanescent wave propagating along the direction x with a positive phase/group velocity. The second branch corresponds to another evanescent wave propagating in the opposite direction along x. For the $y > 0$ semi-infinite plate, we need to have both λ_1 and λ_2 negative. Otherwise, the amplitude $e^{\lambda_1 y} - e^{\lambda_2 y}$ would grow exponentially instead of decaying away from the zero displacement boundary. For the $y < 0$ semi-infinite plate, we need to have both λ_1 and λ_2 positive. Otherwise, the amplitude $e^{\lambda_1 y} - e^{\lambda_2 y}$ would not decay away from the zero displacement boundary. We can, therefore, rewrite Eq. (14) as

$$\lambda_1 + \lambda_2 = +\frac{C}{B} \quad \text{for } y > 0, \tag{15a}$$

$$\lambda_1 + \lambda_2 = -\frac{C}{B} \quad \text{for } y < 0. \tag{15b}$$

Inserting Eq. (14c) into Eq. (14b) results in

$$\lambda_1\lambda_2 = \frac{M}{B} - k_x^2, \tag{16}$$

with $-\sqrt{\frac{M}{B}} < k_x < \sqrt{\frac{M}{B}}$ to ensure the positiveness of the product $\lambda_1\lambda_2$.

For $y > 0$, combining Eqs. (15a) and (16) gives

$$\lambda_1 = \frac{C}{2B} \pm \frac{1}{2}\sqrt{\left(\frac{C}{B}\right)^2 - 4\left(\frac{M}{B} - k_x^2\right)}, \tag{17a}$$

$$\lambda_2 = \frac{C}{2B} \mp \frac{1}{2}\sqrt{\left(\frac{C}{B}\right)^2 - 4\left(\frac{M}{B} - k_x^2\right)}. \tag{17b}$$

Note that the two pairs of evanescent solutions given by Eqs. (17a) and (17b) are equivalent upon permutation of indices 1 and 2, that is, to within a global sign (or global π phase) in Eq. (11).

For $y > 0$, we find two equivalent pairs,

$$\lambda_1 = -\frac{C}{2B} \pm \frac{1}{2}\sqrt{\left(\frac{C}{B}\right)^2 - 4\left(\frac{M}{B} - k_x^2\right)}, \tag{18a}$$

$$\lambda_2 = -\frac{C}{2B} \mp \frac{1}{2}\sqrt{\left(\frac{C}{B}\right)^2 - 4\left(\frac{M}{B} - k_x^2\right)}. \tag{18b}$$

There is, therefore, one single solution of the form given by Eq. (10) for each semi-infinite plate ($y > 0$ or $y < 0$). Each of these solutions correspond to one of the dispersion branches, $\omega = \pm Ck_x$. The $y > 0$ and the $y < 0$ edge mode propagate in opposite directions. This is the signature of counter-propagating helical edge states along the boundary $y = 0$.

The edge mode branches $\omega = \pm Ck_x$ intersect the bulk band given by Eq. (8) at $k_y = 0$, when $k_x^2 = \frac{M}{B}$ (i.e., region of positiveness of the product $\lambda_1\lambda_2$ as seen before). This is illustrated in Fig. 2.

The penetration depth of the edge modes in the direction y for both semi-infinite plates is determined by the smaller in absolute value of λ_1 and λ_2.

We also note that we have limited our investigation to edge states under zero displacement conditions, $\boldsymbol{u}(x, y = 0, \omega) = 0$, along a line transecting the plate. Other type of boundary conditions along the $y = 0$ line, such as clamp condition, namely, $\boldsymbol{u} = 0$ and $\frac{\partial \boldsymbol{u}}{\partial y} = 0$, would lead to seeking solutions with amplitude taking the form $e^{\lambda_1 y} + e^{\lambda_2 y} - e^{-\lambda_1 y} - e^{-\lambda_2 y}$. Under roller conditions, the displacement is not zero anymore but only $\frac{\partial \boldsymbol{u}}{\partial y} = 0$ along the $y = 0$ line, and we would seek amplitudes in the form $a(e^{\lambda_1 y} + e^{-\lambda_1 y}) + b(e^{\lambda_2 y} - e^{-\lambda_2 y})$, where a and b are coefficients to be determined. In these two cases, the displacement increases indefinitely and unphysically away from the zero displacement boundary.

We now apply the method described above to revealing edge modes at the zero displacement edges of a strip. For this, zero displacement boundary conditions are imposed to the plate along lines oriented parallel to the direction x at $y = -\frac{L}{2}$ and $y = +\frac{L}{2}$ forming a strip of width L (Fig. 3).

We seek solutions $\boldsymbol{u} = \begin{pmatrix} u_1(\lambda_1 y, \lambda_2 y) \\ u_2(\lambda_1 y, \lambda_2 y) \end{pmatrix} e^{ik_x x} e^{i\omega t}$ such that $u_1\left(\frac{\pm\lambda_1 L}{2}, \frac{\pm\lambda_2 L}{2}\right) = 0$ and $u_2\left(\frac{\pm\lambda_1 L}{2}, \frac{\pm\lambda_2 L}{2}\right) = 0$. For this, we consider that u_1 and u_2 will be composed of linear combinations of functions of the form: $v(y) = ae^{\lambda_1 y} + be^{-\lambda_1 y} + ce^{\lambda_2 y} + de^{-\lambda_2 y}$. The two equations $v(\pm L/2) = 0$ can be set into the system of equations $\begin{pmatrix} ae^{-\lambda_1 L/2} + be^{+\lambda_1 L/2} & ce^{-\lambda_2 L/2} + de^{+\lambda_2 L/2} \\ ae^{+\lambda_1 L/2} + be^{-\lambda_1 L/2} & ce^{+\lambda_2 L/2} + de^{-\lambda_2 L/2} \end{pmatrix} \begin{pmatrix} 1 \\ 1 \end{pmatrix} = \begin{pmatrix} 0 \\ 0 \end{pmatrix}$. Since the matrices $\begin{pmatrix} 1 & -1 \\ 1 & -1 \end{pmatrix}$ and $\begin{pmatrix} -1 & 1 \\ 1 & -1 \end{pmatrix}$ satisfy this system of equations, we can solve for a, b, c, and d in these two cases, leading to symmetric forms: $v^+(y) = \frac{\cosh\lambda_1 y}{\cosh\lambda_1 L/2} - \frac{\cosh\lambda_2 y}{\cosh\lambda_2 L/2}$ and antisymmetric forms: $v^-(y) = \frac{\sinh\lambda_1 y}{\sinh\lambda_1 L/2} - \frac{\sinh\lambda_2 y}{\sinh\lambda_2 L/2}$. We, therefore, choose the ansatz

$$u_1(y) = \alpha_+ v^+(y) + \alpha_- v^-(y), \tag{19a}$$

$$u_2(y) = \beta_+ v^+(y) + \beta_- v^-(y). \tag{19b}$$

We solve for the four unknown coefficients α_+, α_-, β_+, and β_- by inserting Eqs. (19a) and (19b) into Eq. (6) for $y = -\frac{L}{2}$ and $y = +\frac{L}{2}$. This leads to the eigenvalue problem,

$$\begin{pmatrix} -X & -X & -Y & -Z \\ Y & Z & X & X \\ -X & X & Y & -Z \\ -Y & Z & X & -X \end{pmatrix} \begin{pmatrix} \alpha_+ \\ \alpha_- \\ \beta_+ \\ \beta_- \end{pmatrix} = 0, \tag{20}$$

where $X = B(\lambda_1^2 - \lambda_2^2)$, $Y = C(\lambda_1 T_1 - \lambda_2 T_2)$, and $Z = \left(\lambda_1 \frac{1}{T_1} - \lambda_2 \frac{1}{T_2}\right)$ and $T_1 = \tanh \lambda_1 L/2$ and $T_2 = \tanh \lambda_2 L/2$. There are nontrivial solutions if the determinant of the matrix in Eq. (20) is zero, that is

$$\frac{T_1}{T_2} + \frac{T_2}{T_1} = \frac{C^2\left(\lambda_1^2 + \lambda_2^2\right) - B^2\left(\lambda_1^2 - \lambda_2^2\right)^2}{C^2\lambda_1\lambda_2}. \tag{21}$$

In the limit of large L, the left-hand side of Eq. (21) equals 2 irrespective of the value of λ_1 and λ_2. Eq. (21) reduces to Eq. (14a), namely, the condition for the semi-infinite plate.

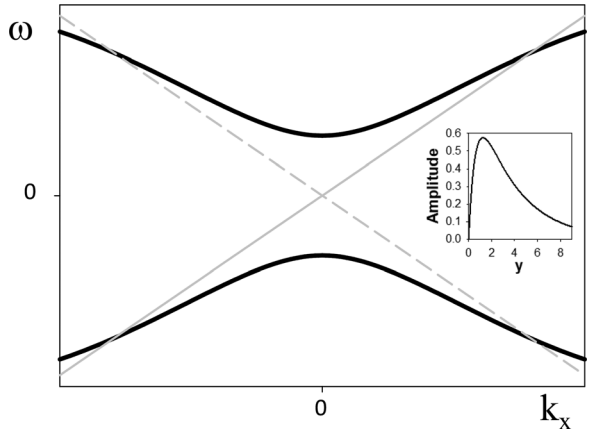

FIG. 2. Schematic illustration of the bulk bands at $k_y = 0$ and $\omega = \pm Ck_x$ bands corresponding to the edge modes at $y = 0$. The inset illustrates schematically the amplitude $(e^{\lambda_1 y} - e^{\lambda_2 y})$ for $y > 0$ with λ_1 and λ_2 given by Eqs. (18a) and (18b). We have chosen $\frac{C}{2B} = 1$, $\frac{M}{B} = 1$, and $k_x^2 = 0.5$.

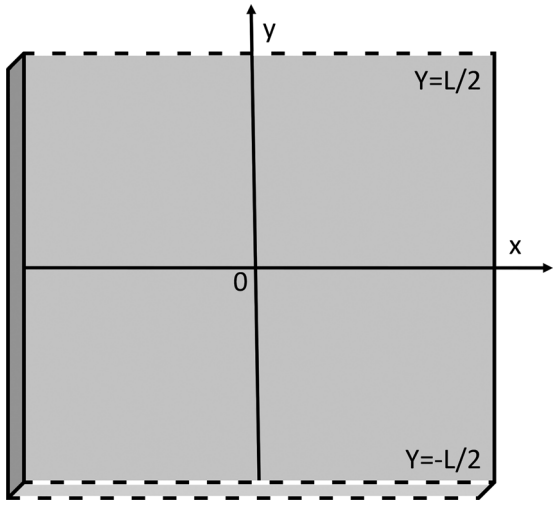

FIG. 3. Schematic illustration of the strip. The dashed line indicates the zero displacement boundaries at $y = -\frac{L}{2}$ and $y = +\frac{L}{2}$. The plate is infinite in the x direction.

Finally, let us consider the appearance of edge modes in the general case of Eq. (21). For this, we rewrite this equation in the form,

$$G(X,Y) = XY\left(\frac{\tanh X/2}{\tanh Y/2} + \frac{\tanh X/2}{\tanh Y/2}\right) - \left(X^2 + Y^2 - \frac{B^2}{C^2L^2}(X^2 - Y^2)^2\right) = 0 \quad (22)$$

with the unknown quantities $X = \lambda_1 L$ and $Y = \lambda_2 L$. There is trivial solution when $X = Y$, or $\lambda_1 = \lambda_2$. This trivial solution corresponds to zero amplitude displacements, i.e., $v^+(y) = 0$ and $v^-(y) = 0$. However, there also exist nontrivial edge mode solutions. In Fig. 4, we have plotted $G(X, Y)$ for $X = \pm 1$ and $\frac{B^2}{C^2L^2} = 0.05$. We note the presence of the corresponding trivial solutions at $Y = X = \pm 1$. The nontrivial solutions arise around $Y = \pm 2.3$.

For small, L, that is the larger $\frac{B^2}{C^2L^2}$, only the trivial solutions survive. Note in Fig. 4 that the solutions for λ_2 may switch from values that are smaller than λ_1 to larger than λ_1, thus determining the depth of the edge mode. The trivial solutions correspond to a maximum, saddle point, or minimum of the function $G(1, Y)$.

We can use Eq. (10) to rewrite the dispersion relations for the evanescent modes as

$$\omega^2 = B^2k_x^4 + A^2k_x^2 + M^2 - B^2\lambda_1^2\lambda_2^2. \quad (23)$$

For each possible pair of λ_1 and λ_2, Eq. (2) shows that the dispersion relation of the corresponding edge mode exhibits a bandgap at the origin, $k_x = 0$. Only in the limit of large L, does Eq. (16) applies an expression (23) reduces to the dispersion of un-gapped edge modes: $\omega^2 = C^2k_x^2$. Therefore, the edge modes may overlap in the finite space of the strip and interact with each other to produce a gap in their spectrum. This is isomorphic to the finite size effects on edge states in quantum spin Hall systems.[30]

We have shown that Dirac factorization can be used to expose the possible topological properties of 2D elastic wave equations. In particular, the nonsymmetry breaking equation for elastic waves in a stiff plate coupled to a rigid substrate is shown to hide spin-like degrees of freedom associated with a gapped band structure. In plates with zero displacement edges such as semi-infinite plates or strips, the Dirac-like elastic wave equation shows the possibility of counter-propagating helical edge modes that may lead to a suppression of backscattering. Immunity to backscattering would require (a) counter-propagating edge modes associated with orthogonal degrees of freedom and that (b) scatterers cannot mix these degrees of freedom. The first condition is approached in the limit of the semi-infinite plate. In the case of strips, the finite size leads to overlap between edge modes which opens a gap in their spectrum eliminating the spin Hall-like effects. The investigation of the effect of the structure or symmetry of scatterers on edge modes will be the subject of future work.

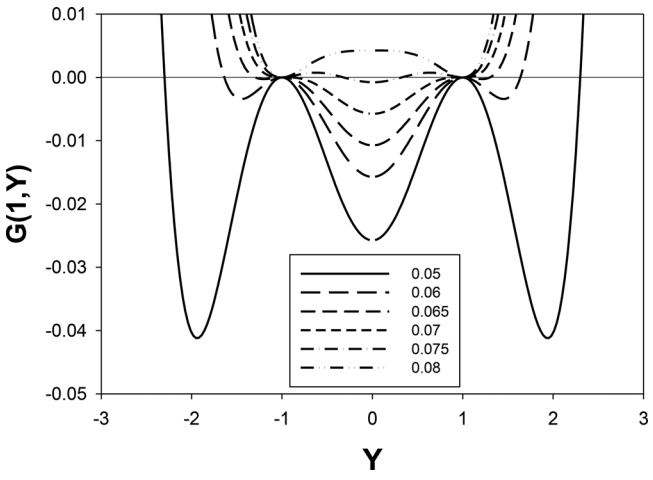

FIG. 4. Plot of $G(X, Y) = 0$ and $X = \pm 1$ and $\frac{B^2}{C^2L^2} = 0.05$, 0.06, 0.065, 0.07, 0.075, and 0.08. Trivial solutions occur at $Y = X$. The solutions different from $Y = \pm 1$ correspond to edge modes.

Dirac factorization tells us only what solutions of the elastic wave equation would be if we could break some symmetry. To fully reveal the possible topological attributes of elastic waves, one would need to apply perturbations in the form of symmetry breaking structural features or externally apply fields. In the first case, one may consider non-homogeneous plates composed of materials with different elastic properties, which geometry and structure break parity symmetry. In the second case, one may modulate in space and time some of the elastic properties of the plate to create synthetic gauge fields (i.e., fields affecting the elastic pseudospin in a way similar to that of a magnetic field applied onto an electron).[22]

Finally, by showing how to break reciprocity in supported stiff plates, this theoretical study provides a roadmap for enabling fundamental functionalities for radio frequency (RF) devices. Acoustic signals offer several advantages in RF mobile communication technologies because of their small wavelengths and high quality factor compared to electromagnetic devices. Topological acoustics insulators may enable implementation of guided-wave technologies in RF acoustic wave devices over broad frequency ranges with reduced losses from defects, disorder, and sharp angles.[1]

This research was funded by the National Science Foundation Emerging Frontiers in Research and Innovation (EFRI) Award (No. 1640860). P.A.D. acknowledges useful communications with Dr. Shunqing Shen.

AUTHOR DECLARATIONS

Conflict of Interest

The authors declare no competing interests.

DATA AVAILABILITY

The data that support the findings of this study are available from the corresponding author upon reasonable request.

REFERENCES

[1]A. Alù, C. Daraio, P. A. Deymier, and M. Ruzzene, "Topological acoustics," Phys. Today **17**(3), 13 (2021).
[2]G. Ma, M. Xiao, and C. T. Chan, "Topological phases in acoustic and mechanical systems," Nat. Rev. Phys. **1**, 281 (2019).
[3]J. Yin, M. Ruzzene, J. Wen *et al.*, "Band transition and topological interface modes in 1D elastic phononic crystals," Sci. Rep. **8**, 6806 (2018).
[4]M. A. Hasan, L. Calderin, P. Lucas *et al.*, "Spectral analysis of amplitudes and phases of lattice vibrations: Topological applications," J. Acoust. Soc. Am. **146**, 748 (2019).

[5]R. Fleury, D. L. Sounas, and A. Alù, "Subwavelength ultrasonic circulator based on spatiotemporal modulation," Phys. Rev. B **91**, 174306 (2015).
[6]M. Z. Hasan and C. L. Kane, "Topological insulators," Rev. Mod. Phys. **82**, 3045 (2010).
[7]N. Swinteck, S. Matsuo, K. Runge *et al.*, "Bulk elastic waves with unidirectional backscattering-immune topological states in a time-dependent superlattice," J. Appl. Phys. **118**, 063103 (2015).
[8]G. Trainiti and M. Ruzzene, "Non-reciprocal elastic wave propagation in spatiotemporal periodic structures," New J. Phys. **18**, 083047 (2016).
[9]Y. Chen, X. Li, H. Nassar *et al.*, "Nonreciprocal wave propagation in a continuum-based metamaterial with space-time modulated resonators," Phys. Rev. Appl. **11**, 064052 (2019).
[10]P. A. Deymier, V. Gole, P. Lucas *et al.*, "Tailoring phonon band structures with broken symmetry by shaping spatiotemporal modulations of stiffness in a one-dimensional elastic waveguide," Phys. Rev. B **96**, 064304 (2017).
[11]P. Wang, L. Lu, and K. Bertoldi, "Topological phononic crystals with one-way elastic edge waves," Phys. Rev. Lett. **115**, 104302 (2015).
[12]R. K. Pal, M. Schaeffer, and M. Ruzzene, "Helical edge states and topological phase transitions in phononic systems using bi-layered lattices," J. Appl. Phys. **119**, 084305 (2016).
[13]R. K. Pal and M. Ruzzene, "Edge waves in plates with resonators: An elastic analogue of the quantum valley Hall effect," New J. Phys. **19**, 025001 (2017).
[14]H. Ge, X. Ni, Y. Tian *et al.*, "Experimental observation of acoustic Weyl points and topological surface states," Phys. Rev. Appl. **10**, 014017 (2018).
[15]F. Li, X. Huang, J. Lu *et al.*, "Weyl points and Fermi arcs in a chiral phononic crystal," Nat. Phys. **14**, 30 (2018).
[16]M. Xiao, W.-J. Chen, W.-Y. He *et al.*, "Synthetic gauge flux and Weyl points in acoustic systems," Nat. Phys. **11**, 920 (2015).
[17]S. S. Ganti, T.-W. Liu, and F. Semperlotti, "Weyl points and topological surface states in a three-dimensional elastic lattice," New J. Phys. **22**, 083001 (2020).
[18]P. A. M. Dirac, "The quantum theory of the electron," Proc. R. Soc. London, Ser. A **117**, 610 (1928).
[19]W. Gerlach and O. Stern, "Der experimentelle Nachweis der Richtungsquantelung im Magnetfeld," Z. Phys. **9**, 349 (1922).
[20]P. Deymier and K. Runge, *Sound Topology, Duality, Coherence and Wave Mixing: An Introduction to the Emerging New Science of Sound* (Springer International Publishing, 2017).
[21]P. A. Deymier, K. Runge, N. Swinteck *et al.*, "Torsional topology and fermion-like behavior of elastic waves in phononic structures," C. R. Méc. **343**, 700 (2015).
[22]P. Deymier and K. Runge, "One-dimensional mass-spring chains supporting elastic waves with non-conventional topology," Crystals **6**, 44 (2016).
[23]P. A. Deymier, K. Runge, J. O. Vasseur *et al.*, "Elastic waves with correlated directional and orbital angular momentum degrees of freedom," J. Phys. B **51**, 135301 (2018).
[24]P. A. Deymier, J. O. Vasseur, K. Runge *et al.*, "Separability and non-separability of elastic states in arrays of one-dimensional elastic waveguides," in *Phonons in Low-Dimensional Structure*, edited by V. N. Stavrou (InTech Open, 2018), Chap. 3.
[25]S. Timoshenko, *History of Strength of Materials* (McGraw-Hill, New York, 1953).
[26]A. E. H. Love, "The small free vibrations and deformation of a thin elastic shell," Philos. Trans. R. Soc. London, Ser. A **179**, 491–549 (1888).
[27]J. Hladik, *Spinors in Physics*, translated by J. M. Cole (Springer, 1999).
[28]X.-L. Qi, Y.-S. Wu, and S.-C. Zhang, "Topological quantization of the spin Hall effect in two-dimensional paramagnetic semiconductors," Phys. Rev. B **74**, 085308 (2006).
[29]J. K. Asbóth, L. Oroszlány, and A. Pályi, "A short course on topological insulators: Band structure and edge states in one and two dimensions," in *Lecture Notes in Physics* (Springer, 2016), Vol. 919, p. 85.
[30]B. Zhou, H.-Z. Lu, and R.-L. Chu *et al.*, "Finite size effects on helical edge states in a quantum spin-hall system," Phys. Rev. Lett. **101**, 246807 (2008).